

Many-body localization enables iterative quantum optimization

Hanteng Wang,^{1,2,*} Hsiu-Chung Yeh,¹ and Alex Kamenev^{1,3,†}

¹*School of Physics and Astronomy, University of Minnesota, Minneapolis, Minnesota 55455, USA*

²*Shanghai Center for Complex Physics, School of Physics and Astronomy,
Shanghai Jiao Tong University, Shanghai 200240, China*

³*William I. Fine Theoretical Physics Institute, University of Minnesota, Minneapolis, Minnesota 55455, USA*
(Dated: November 2, 2021)

We suggest an iterative quantum protocol, allowing to solve optimization problems with a glassy energy landscape. It is based on a periodic cycling around the tricritical point of the many-body localization transition. This ensures that each iteration leads to a non-exponentially small probability to find a lower local energy minimum. The other key ingredient is to tailor the cycle parameters to a currently achieved optimal state (the “reference” state) and to reset them once a deeper minimum is found. We show that, if the position of the tricritical point is known, the algorithm allows to approach the absolute minimum with any given precision in a polynomial time.

Optimization problems are ubiquitous [1, 2]. A large subclass of them is discrete optimization tasks, which may be mapped onto spin models with the optimal solution being a ground state of a certain classical spin Hamiltonian. The optimization problems are hard due to the spin-glass phase [3–5], i.e. presence of multiple local minima in the energy landscape of the corresponding model. The idea of utilizing quantum tunneling in order to facilitate transitions between these local minima was coined a long time ago. Probably the earliest and most transparent way of doing it is realized via the adiabatic quantum annealing (QA) procedure [6–8]. Its bottleneck is associated with exponentially small energy gaps between instantaneous energy levels of the corresponding *quantum* Hamiltonian [9–15]. Those lead to Landau-Zener transitions [16–18], which take the system out of its adiabatic ground state. As a result in order to succeed, the QA should be performed exponentially slow.

This stimulates interest in constructing approximate *diabatic* protocols [19, 20], collectively known as quantum approximate optimization algorithms [21–24]. The idea is to force the system to gradually approach its GS with a relatively fast running cycles [25–28].

Here we suggest an iterative quantum algorithm which runs along a closed cycle in a space of parameters. The key observation is that the cycle must encircle a tricritical point of the many-body localization (MBL) [29–37] transition. The three phases coming together at the tricritical point are the spin-glass, the MBL paramagnet and the delocalized paramagnet. The cycle starts in the spin-glass and goes successively into MBL and delocalized paramagnets before returning back to the spin-glass, where the projective measurement is performed. We show that iterations of such cycle lead to a systematic decrease of energy of the measured state. The cycle duration and a number of required cycles scale algebraically

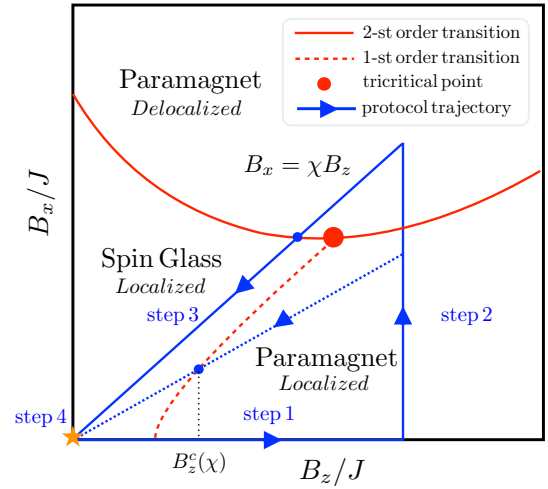


FIG. 1. **Phase diagram and the protocol.** Phase diagram of the Hamiltonian (3) for a specific reference state. Full red line indicates a 2-nd order transition [38] between MBL and delocalized paramagnet; the dashed red line is the 1-st order transition between the glass and MBL paramagnet. They meet at the tricritical point. The blue lines with arrows represent one optimization cycle. The dotted blue line is a subcritical slope, $\chi < \chi_c$, which most likely brings the system back to the initial reference state.

with the system size. Given a desired precision of the optimization, the cycle trajectory should pass increasingly close to the tricritical point.

The iterative optimization has already appeared in the literature, see e.g. Refs. [25–28]. We found it useful to combine it with the idea of the reference Hamiltonian [39–41]. The latter calls for using a control parameter (eg. a longitudinal magnetic field) which is collinear with a local Bloch sphere direction of the individual qubits. This leads to an adjustment of the cycle parameters according to a result of the measurement taken at the end of the previous cycle. We show that such strategy allows to navigate the system arbitrarily close to the MBL tricritical point, as required by the proposed

* wanhanteng@sjtu.edu.cn

† kamenev@physics.umn.edu

algorithm. As an example of optimization in a spin-glass system, we use Sherrington-Kirkpatrick (SK) model [42], whose MBL properties are discussed Refs. [34–37].

Results

Iterative quantum optimization protocol. As an example of an optimization problem with a glassy landscape we choose a realization of the Sherrington-Kirkpatrick (SK) model [42] specified by a Hamiltonian

$$H_{\text{SK}} = \sum_{ij} J_{ij} \sigma_i^z \sigma_j^z. \quad (1)$$

Here σ_i^z are z -Pauli matrices, which represent binary optimization parameters, labeled by $i = 1, 2, \dots, N$. The cost function is chosen to be quadratic in these parameters given by a cost matrix, J_{ij} . In our examples its matrix elements are taken from independent Gaussian distributions with zero mean and variance J^2/N . Eigenstates of the Hamiltonian, denoted as $\alpha = 1, 2, \dots, 2^N$, are encoded by bit-strings, $\{s_i^\alpha\}$, with $s_i^\alpha = \pm 1$ showing “up” or “down” polarization of the i -th spin. The corresponding eigenenergies are $E_\alpha = \sum_{ij} J_{ij} s_i^\alpha s_j^\alpha$. Since all the terms in the Hamiltonian (1) commute with each other, the problem is purely classical.

It is known [5, 43, 44] that E_α form a glassy landscape with exponentially many local minima (i.e. states such that flipping *any* one (or even a few) spins results in energy being increased). Simulated classical annealing is typically trapped into one of such local minima. The local minima are separated from each other by the *Hamming distance* of the order N spin flips. The goal of the optimization is to find progressively deeper local minima, eventually hitting the global one.

The conventional adiabatic QA procedure calls for modifying the Hamiltonian (1) to add non-commutative (aka quantum) terms. The simplest of such quantum terms is (in general time-dependent) magnetic field applied in the x -direction:

$$H(t) = H_{\text{SK}} + B_x(t)H_q, \quad H_q = -\sum_{i=1}^N \sigma_i^x. \quad (2)$$

If the x -magnetic field is initiated to be large, $B_x \gg J$, the ground state is close to all spins being polarized in the x -direction [34, 35]. Such ground state is separated by a large gap, $\sim B_x$, from the rest of the spectrum. Cooling the system down to a temperature $T \ll B_x$ puts it almost surely in its true ground state. One then slowly decreases $B_x(t)$ down to zero so that the Hamiltonian goes back to the pure SK model (1). If this process is adiabatic, the state of the system follows its instantaneous ground state and arrives at the global SK minimum. For the system to *not* undergo any Landau-Zener transition, the annealing rate should be $\tau_{\text{anneal}}^{-1} \ll \Delta_{\text{min}}^2/B_x$, where Δ_{min} is a minimal avoiding crossing gap, encountered

by the ground state. As argued in Refs. [9–11] some of these gaps are exponentially small, demanding an exponentially long annealing time, τ_{anneal} .

Hereby we suggest an iterative cyclic algorithm capable of systematically approaching the ground state, while not being exponentially slow. Before the first cycle starts one performs a simulated classical annealing, arriving at one of the local minima, which we’ll call a reference state, $\{s_i^r\}$. Each cycle consists of the four successive steps summarized in Fig. 1:

Step 1. The qubit array is initialized to the reference state and is programed to represent the following Hamiltonian

$$H(t) = H_{\text{SK}} + B_x(t)H_q + B_z(t)H_{\text{ref}}^r, \quad (3)$$

where the z -field in the reference Hamiltonian is tailor-made to be co-directed with all the spins of the given reference bit-string, $\{s_i^r\}$,

$$H_{\text{ref}}^r = -\sum_i s_i^r \sigma_i^z. \quad (4)$$

One starts from the pure SK model, $B_x = B_z = 0$, and then increases $B_z(t)$ from zero passing the critical field B_z^c , separating the spin-glass phase from the paramagnet. Since $B_x = 0$ in step 1, the Hamiltonian is purely classical and the system remains in the reference state, no matter how fast B_z is increased. In fact, all the states remain to be pure bit-strings of H_{SK} , but their relative energies do change. The H_{ref}^r is chosen in a way to push the energy of the reference state sharply down: $E_r(B_z) = E_r(0) - NB_z$. The other local minima are far in the Hamming distance from the reference state and thus evolve typically as $E_\alpha(B_z) = E_\alpha(0) \pm \sqrt{N}B_z$. As a result, soon enough the reference state is the unique ground state, separated by the gap. This first happens at the critical field B_z^c .

Step 2: B_x is increased while B_z is fixed. The gap in the paramagnetic phase is proportional to the total magnetic field $\sqrt{B_x^2 + B_z^2}$, and is independent of the system size. One does not need an exponential or even a power law (in system size) long time to increase B_x while keeping the system in the ground state of the full Hamiltonian (3). However, since the full Hamiltonian is now quantum, its ground state is a superposition of many bit-string states. The B_x is increased until it reaches a certain ratio with the z -field: $\chi = B_x/B_z$.

Step 3: Decreasing B_z and B_x keeping the fixed ratio χ between them. Along this path the system again crosses the phase boundary between the paramagnetic and the glassy phases. This boundary is marked by the first avoiding crossing transition between the ground state and the lowest excited state. The size of the corresponding gap strongly depends on the slope χ , which we discuss in detail in the next section. The upshot is that Landau-Zener transitions may occur during this part of the cycle,

but with an overwhelming probability they leave the system in a state with an energy, which is lower than that of the initial reference state. The main danger is that the system remains in the reference state. This may be avoided, however, by a careful choice of the slope χ .

Step 4. After both B_x and B_z reach zero in the end of the step 3, the system ends up in a superposition state. Now the measurement of each qubit is performed and the state collapses to a certain bit-string. Starting from this measured bit-string, the simulated annealing leads the system down to a nearest local minimum. If the energy of this new local minimum is less than that of the reference state, it is taken as the new reference state and the cycle is repeated from step 1. If, however, its energy is larger or the same, the system is initiated back to the old reference state and the cycle is again repeated from step 1.

Three key features of this protocol qualitatively improve its performance vis-a-vis the conventional QA. First, the reference state is iteratively set to be the minimal energy local minimum found in all previous trials. This way the reference energy never increases. Second, the choice of the reference Hamiltonian guarantees that Zener transitions in step 3 almost always decrease the energy. Third (and most significant), cycling around the tricritical point of the MBL transition allows to accomplish such energy decrease in a polynomial time. The second and the third items on this list are explained in the next section.

MBL transition and the phase diagram. To illustrate the statements made above, consider Fig. 2 depicting schematically the adiabatic spectrum of the Hamiltonian (3) vs. B_z for several fixed slopes χ , such that $B_x = \chi B_z$. Figure 2a shows $\chi = 0$ case, which corresponds to the step 1 of the protocol. Since $B_x = 0$, the Hamiltonian is classical and there are no transitions between the states. The corresponding energy levels cross each other. The reference Hamiltonian (4) is chosen in a way to ensure that the reference state (red line in Fig. 2a) goes down with a maximal slope. As a result, the reference state is destined to become a ground state at a certain critical field B_z^c . For $B_z > B_z^c$, there is a finite energy gap between the ground reference state and the rest of the spectrum. We thus refer to this phase as the paramagnet. Since all the states of such a paramagnet are represented by pure bit-strings, they are perfectly many-body localized in the bit-string basis. Notice that within the glassy phase, $B_z < B_z^c$, the reference state crosses *only* the states whose SK energy is less than E_r .

Figure 2b shows the spectrum for $\chi < \chi_c$. Due to the presence of H_q , spin flips are allowed leading to avoiding crossings gaps in the spectrum. At small B_x , these gaps are exponentially small, because of typically large (order N) Hamming distance between low-energy local minima. This makes the critical field $B_z^c(\chi)$ to be well defined in

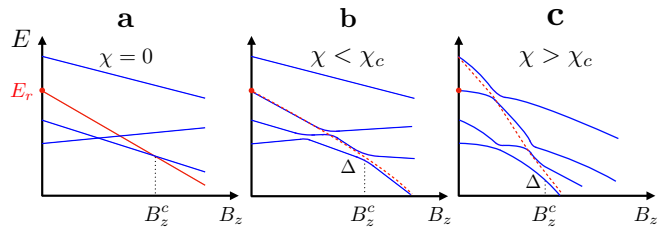


FIG. 2. **Spectrum and Landau-Zener transition.** A sketch of the spectrum of Eq. (3) for different values of the slope $\chi = B_x/B_z$. The red dots represent the SK energy of the reference state. In **a**, the red line depicts the energy of reference state. In **b** and **c**, the reference state is the eigenstate only at $B_z = B_x = 0$. The red dashed line indicates a *diabatic* trajectory of step 3, undergoing Landau-Zener transition (from large B_z to small B_z).

the large N limit. It marks the *first order* transition between MBL glass and MBL paramagnet phases. If the step 3 of the protocol is run (right to left) along this trajectory (dotted blue line in Fig. 1) with a non-exponentially small rate, the state of the system most likely follows the dashed red line. This brings the system back to the initial reference state, making the protocol fail. Notice, however, that in rare cases when the state does follow the adiabatic trajectories, the energy of the system is bound to be *below* the initial energy, E_r .

To increase the probability of adiabatic transitions lowering the energy, the gaps need to be increased. This is achieved by working at $\chi > \chi_c$, Fig. 2c. Such a strategy comes with a steep prize, however. Indeed, the reference state may also hybridize now with higher energy states. This leads to undesirable transitions increasing the energy (dashed red line in Fig. 2c). The question is if one can benefit from energy decreasing adiabatic trajectories, without being handicapped by Zener transitions to higher energy states (the latter phenomenon is responsible for the failure of the conventional QA [9–11, 14, 15]).

To answer this question one needs to examine MBL transition on the phase diagram of our protocol, Fig. 1. Being defined by the Hamiltonian (3), the latter is tight to a specific reference state. Depending on the quantum component B_x , this state and its neighbors may be either localized (small B_x) or delocalized (large B_x) in the bit-string basis. The transition between the two is characterized by a divergent localization-Hamming-length in the many-body Fock (i.e. bit-string) space [29–33]. Therefore the MBL transition is of the 2-nd order [34–36, 38]. It divides the phase space, Fig. 1, onto the two disconnected regions. As explained above, there is also the 1-st order transition between gapless (in the large N limit) spin glass phase and the gaped paramagnet, both within the localized phase. The latter transition is not associated with a divergent Hamming distance. It is reasonable to expect that the 1-st order transition line terminates at a *tricritical* point somewhere along the MBL transition

boundary, Fig. 1.

Position of the tricritical point defines a critical slope χ_c of the step 3 part of the cycle. For $\chi < \chi_c$ the step 3 encounters the 1-st order transition within the MBL phase. Since all states below the reference one are many-body localized, the avoiding crossing gaps are exponentially small. Unless performed adiabatically (i.e. within exponentially long time), the step 3 is bound to bring the system back to its initial reference state.

The situation is qualitatively different for $\chi > \chi_c$. Here the step 3 trajectory passes through the second order transition between a delocalized paramagnet and localized glass phase. There is a divergent localization-Hamming-length on the glass side. This makes the states to be spanned by progressively wider superpositions of bit-strings and thus leads to non-exponential gaps near the MBL transition. Indeed, from generic finite size scaling considerations of the 2-nd order transition, one expects the energy gap near the MBL transition to scale as

$$\Delta \propto \frac{(\chi - \chi_c)^\theta}{N^{\nu z}}, \quad (5)$$

where θ and νz are critical exponents. It was recently argued [14] that in the Hopfield model (a close cousin of SK) $\nu z = 1/3$.

Therefore if the step 3 is performed within the power-law time, $\tau_3 \sim N^{2\nu z}$, it results in a certain number of the avoiding crossing transitions taking the adiabatic turn. Those typically happen at a relatively large $B_x \approx \chi_c B_z^c(\chi_c)$, close to the MBL transition. What remains to be shown is that these transitions indeed lead to a systematic energy decrease, not overshadowed by transitions to the higher energy states, as in Fig. 2c. The key insight is that this may be achieved by tuning the slope χ closer to the critical one from above, $\chi \rightarrow \chi_c^+$.

To show this we numerically isolate local minima states along with their simulated annealing basins of attraction from other local minima basins. One may diagonalize Hamiltonian (3) in each of such basins (details of this procedure are described in Methods section). This way we keep the geometry of the levels, undisturbed by the avoiding crossings generated by tunneling between the local minima. It allows us to track exact identities of all local minima, in particular the reference state. Figure 3 shows energies of such isolated local minima vs. B_z . One can now calculate the number of local minima, with both higher energy, $\mathcal{N}_>$, and lower energy, $\mathcal{N}_<$, crossing the reference state. Figure 4 shows the ratio $\mathcal{N}_>/\mathcal{N}_<$ vs. slope χ . As expected, for $\chi < \chi_c$ there are practically no higher energy states getting in contact with the reference one. On the other hand, the fraction of the higher energy states grows rapidly for $\chi > \chi_c$. The smaller the energy of the reference state the faster this fraction grows. This is expected since for a deep local minimum there aren't too many other local minima below it, but

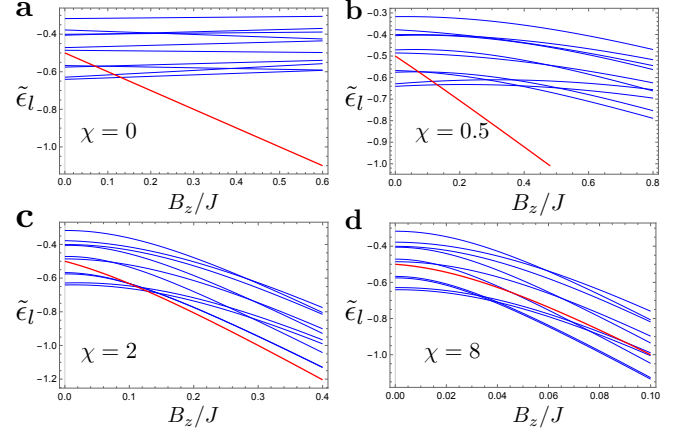


FIG. 3. **Spectra of isolated local minima.** Spectra of isolated local minima, shown in blue, for different χ . The reference state is shown in red. As χ increases, a progressively larger fraction of higher energy states curves down (due to the level repulsion from their local Hamming distance neighborhood) to intersect the reference state.

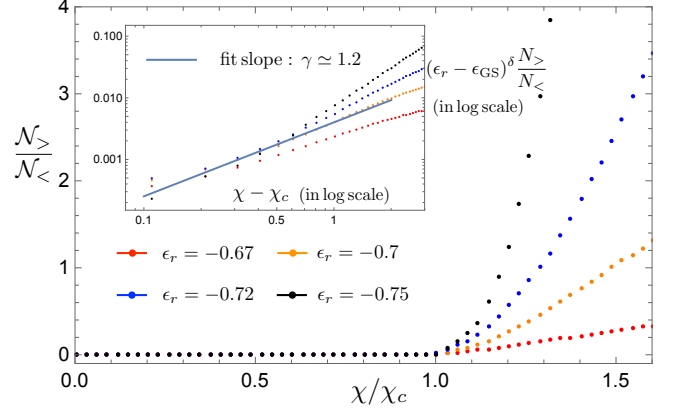


FIG. 4. **States ratio and scaling exponents.** Ratio of higher and lower energy isolated local minima intersecting with the reference state as a function of the slope χ/χ_c . The data is taken for several values of the reference state energy ϵ_r . The ground state energy is $\epsilon_{GS} = -0.8$. Inset: $(\epsilon_r - \epsilon_{GS})^\delta \mathcal{N}_>/\mathcal{N}_<$ vs. $\chi - \chi_c$ in log-log scale; solid line is fitting with Eq. (6).

there are plenty above. The most important lesson from Fig. 4 is what the ratio grows continuously as

$$\frac{\mathcal{N}_>}{\mathcal{N}_<} \propto \frac{(\chi - \chi_c)^\gamma}{(\epsilon_r - \epsilon_{GS})^\delta}, \quad (6)$$

where $\gamma \approx 1.2$ and $\delta \approx 2.0$ are critical exponents and $\epsilon_\alpha = E_\alpha/(NJ)$. The critical slope can depend on the reference state. In our simulations this dependence appears to be very weak, if any, with $\chi_c \approx 3.6$.

Equations (5) and (6) allow to estimate efficiency of the algorithm vis-a-vis its running time, precision and other requirements. First one fixes the desired precision, i.e. deviation from the global minimum: $\delta_\epsilon = \epsilon_r - \epsilon_{GS}$.

For simplicity, let us settle with the regime where every other cycle, in average, results in lowering the energy of the reference state. This amounts to the equal number of upper and lower energy local minima intersections, $\mathcal{N}_>/\mathcal{N}_< = 1$. This dictates that the protocol should be run at $\chi - \chi_c \lesssim \delta_\epsilon^{\delta/\gamma}$. Although it requires a more and more precise knowledge of χ_c , if precision is increased, the good news is that the required $\chi - \chi_c$ does not scale with the system size. We discuss ways of “on the fly” measurement of χ_c in next section.

The running time is given by a number of required cycles, n_c , multiplied by duration of the step 3, τ_3 (steps 1, 2 and 4 are typically faster). The latter is given $\tau_3 \gtrsim \Delta^{-2} \propto N^{2\nu z} \delta_\epsilon^{-2\theta\delta/\gamma}$. Finally, assuming that every successful cycle eliminates a fraction $p < 1$ of remaining lower energy states, one may estimate a number of required cycles as $n_c \sim N/\log(1-p)$. This leads to the total time of the optimization, which scales as

$$\tau = n_c \tau_3 \propto N^{2\nu z + 1} \delta_\epsilon^{-2\theta\delta/\gamma}. \quad (7)$$

It increases with both the system size and the optimization precision, but both dependences are power-laws, rather than exponential.

A recent study [45] argued that SK model complexity scales as $N^2 C(\delta_\epsilon)$, where $C(\delta_\epsilon)$ is a function depending only on the required precision δ_ϵ . Our algorithm can’t do better than this, even if $2\nu z < 1$. Indeed, each cycle includes classical simulated annealing step with the required time $\tau_{sa} \sim N$. This limits the cycle duration (but not the qubit coherence time) by $\max\{\tau_{sa}, \tau_3\}$. Thus the total time scales as $\max\{N^2, N^{2\nu z + 1}\}$. However, the present quantum algorithm can match the performance of Ref. [45], if $2\nu z \leq 1$.

Discussion

We have outlined the quantum approximate optimization algorithm, which is capable of systematically approaching the global minimum of a glass within the power-law (in the system size) time (7). It is based on a variant of the quantum annealing, with the reference state specific Hamiltonian (3) and the iterative cycle encircling the tricritical point of the MBL transition.

An attractive feature of the algorithm is that it does not require an exceedingly long qubit coherence time. Indeed, the projective measurement is done after every cycle. Therefore the required coherence time scales as a period of the single cycle, $\tau_3 \propto N^{2\nu z}$. Moreover, if one or a few qubits produce a faulty readout, it will be automatically corrected by simulated classical annealing, performed after every quantum state measurement. Another advantage is a limited number of the required dynamical control parameters. In fact, after the Hamiltonian (3) is set, all qubits are subject to only two dynamically varying controls: $B_x(t)$ and $B_z(t)$. There is also the measurement step, requiring a simultaneous measurement of all σ_i^z .

The main drawback of the algorithm is that it requires an exceedingly precise knowledge of the MBL tricritical point slope, χ_c , which is, of course, not known apriori for a given specific optimization task. Although this is a concern, there are ways to go about it. First, our simulations indicate that realization specific (and reference state specific) fluctuations of χ_c are small and decrease with increasing N . This means that χ_c can be determined (at least approximately) once for an entire broad class of optimization tasks. Second, the slope may be fine-tuned on the fly, while optimization cycles are running. Indeed, if the slope happens to be subcritical $\chi < \chi_c$, the successive iterations lead back to the same reference state. Once it happens, the slope of the next iteration needs to be somewhat increased. On the other hand, if the slope exceeds the acceptable range $\chi > \chi_c + \delta_\epsilon^{\delta/\gamma}$, the cycles bring the system to the local minima with higher energies. This undesirable outcome is corrected by decreasing the slope. Therefore the imprecise knowledge of χ_c may be compensated by a certain overhead on the number of cycles, n_c .

Methods

Local minima isolation. Here we discuss a phenomenological approach to numerically isolate local minima states along with their simulated annealing basins of attraction from other local minima basins. The low-energy Landau-Zener transitions occur only between the local minima states, $|l\rangle$, due to the fact that local minima are repelled down by their Hamming distance neighbors. To simplify the spectrum in the spin-glass phase, one may identify a basin state $|\tilde{l}\rangle$, which is a wave packet localized at local minimum state $|l\rangle$, i.e. it is a superposition of $|l\rangle$ and its Hamming-neighbor states. Upon simulated annealing, all this states lead to the corresponding local minimum state, i.e. $|\tilde{l}\rangle \rightarrow |l\rangle$. Therefore in the spin-glass phase, one can approximate the spectrum of Eq.(3) by the spectrum of local minima.

A hopping between any two local minima is typically exponentially small, since the Hamming distance is of the order of the system size N . An effective Hamiltonian between two basin states is

$$H_{l,l'}^{\text{block}} = \begin{pmatrix} \tilde{E}_l & t_{ll'} \\ t_{ll'} & \tilde{E}_{l'} \end{pmatrix}, \quad (8)$$

where $t_{ll'}$ is the effective hopping between l and l' basin states with energy \tilde{E}_l and $\tilde{E}_{l'}$, which is renormalized by the Zeeman effect of B_z and by repulsion from local Hamming neighborhood due to B_x , i.e.

$$\tilde{E}_l = E_l + \Sigma_l(B_z, B_x). \quad (9)$$

Here $\Sigma_l(B_z, B_x)$ is the self-energy which gives the energy curves $\tilde{\epsilon}_l = \tilde{E}_l/(NJ)$ of Fig. 3 without the anti-crossing effect.

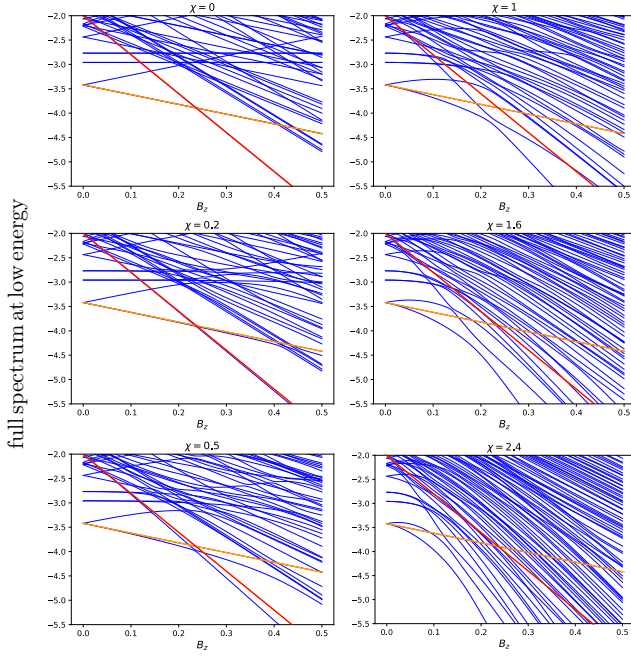


FIG. 5. **Exact diagonalization.** Low energy spectra of Eq. (3) for different χ . System size is $N = 10$. Red and orange straight lines are the reference and ground-state energies, correspondingly at $\chi = 0$. They are repeated on all panels as a guide for eye. When $\chi = 0$, energies are straight lines with slopes (11). For larger χ , energies are curved down, due to the level repulsion. Simultaneously the gaps open up.

By analyzing a small system size exact diagonalization, shown in Fig. 5, we found that the self-energy is well approximated by

$$\Sigma_l(B_z, B_x) = NJ \left[f_l - \sqrt{(f_l + m_l B_z/J)^2 + (B_x/J)^2} \right], \quad (10)$$

where m_l and f_l are basin dependent phenomenological parameters discussed below. This expression interpolates between the limiting cases of $\chi \ll 1$ and $\chi \gg 1$. For $\chi \ll 1$ one may put $B_x = 0$, finding $\Sigma_l = -m_l N B_z$. The corresponding slope, m_l , for a given local minimum l measures the spin configuration overlap with the reference state r :

$$m_l = \frac{1}{N} \sum_{i=1}^N s_i^l \cdot s_i^r = 1 - 2d_l/N, \quad (11)$$

where d_l is the Hamming distance from the reference state to the basin l . We found that d_l 's are distributed according to a binomial distribution

$$P(d_l) = \frac{1}{2^N} \binom{N}{d_l}, \quad (12)$$

which is natural, if one assumes totally random spin flip-ping (or not) to reach another local minimum.

For $\chi \gg 1$, one may start assuming $B_z = 0$. At $B_x/J \ll 1$, Eq. (10) is approximate by

$$\Sigma_l \approx -NB_x^2/(2f_l J). \quad (13)$$

This may be viewed as a result of the second order, in B_x , perturbation of the SK model. The energy of the local minimum goes down due to the level repulsion and the second order perturbation comes from the one-spin flip states. The factor $1/(2f_l J)$ describes the average inverse energy difference between the local minimum and one-spin flip states. The distribution of f_l 's is approximated by a uniform box in the interval $1/4 < f_l < 3/4$. Finally at $B_x \gg J$, the system is fully polarized with $\Sigma_l \approx -NB_x$. Equation (10) is the simplest way to interpolate between all these limits, which works extremely well for small system size simulations.

To perform larger system size simulations, leading to Fig. 4, we statistically generate multiple local minima energy curves according to Eqs. (9)–(13). The distribution of SK local energies, E_l is taken from Refs. [43 and 44] and is assumed to be statistically independent from the other random parameters, m_l and f_l . We simulated system sizes up to $N = 200$ and verified that the qualitative features of Fig. 4 are robust against variations in specific distributions of the random parameters. The first order (red dashed) line in Fig. 1 is determined by the position of $(B_z^c(\chi), \chi B_z^c(\chi))$ for a fixed reference state, while $B_z^c(\chi)$ is given by the last intersection of the reference state.

Acknowledgement

This work was supported by the NSF grant DMR-2037654.

Author contributions

All authors participated in developing the theory. H.W., and H.-C.Y. performed the analysis of numerical simulation. A.K. conceived and supervised the project. All authors contributed significantly to the writing of the manuscript.

-
- [1] M. R. Garey and D. S. Johnson, *Computers and Intractability: A Guide to the Theory of NP-Completeness* (W. H. Freeman & Co., New York, 1979).
 - [2] S. Arora and B. Barak, *Computational Complexity: A Modern Approach* (Cambridge University Press, Cambridge, UK, 2009).
 - [3] F. Barahona, On the computational complexity of Ising spin glass models, *J. Phys. A: Math. Gen.* **15**, 3241 (1982).
 - [4] A. Lucas, Ising formulations of many NP problems, *Frontiers Phys.* **2**, 5 (2014).
 - [5] M. Mézard, G. Parisi, and M. A. Virasoro, *Spin Glass Theory and Beyond* (World Scientific, Singapore, 1987).

- [6] T. Kadowaki and H. Nishimori, Quantum annealing in the transverse Ising model, *Phys. Rev. E* **58**, 5355 (1998).
- [7] E. Farhi, J. Goldstone, S. Gutmann, and M. Sipser, Quantum computation by adiabatic evolution, (2000), [arXiv:quant-ph/0001106](#).
- [8] E. Farhi, J. Goldstone, S. Gutmann, J. Lapan, A. Lundgren, and D. Preda, A quantum adiabatic evolution algorithm applied to random instances of an np-complete problem, *Science* **292**, 472 (2001).
- [9] M. H. Amin and V. Choi, First-order quantum phase transition in adiabatic quantum computation, *Phys. Rev. A* **80**, 062326 (2009).
- [10] B. Altshuler, H. Krovi, and J. Roland, Anderson localization makes adiabatic quantum optimization fail, *Proc. Natl. Acad. Sci. U.S.A.* **107**, 12446 (2010).
- [11] T. Jörg, F. Krzakala, J. Kurchan, A. C. Maggs, and J. Pujos, Energy gaps in quantum first-order mean-field-like transitions: The problems that quantum annealing cannot solve, *Europhys. Lett.* **89**, 40004 (2010).
- [12] T. Jörg, F. Krzakala, J. Kurchan, and A. Maggs, Simple Glass Models and Their Quantum Annealing, *Phys. Rev. Lett.* **101**, 147204 (2008).
- [13] S. Knysh and V. Smelyanskiy, On the relevance of avoided crossings away from quantum critical point to the complexity of quantum adiabatic algorithm, (2010), [arXiv:1005.3011](#).
- [14] S. Knysh, Zero-temperature quantum annealing bottlenecks in the spin-glass phase, *Nat. Commun.* **7**, 12370 (2016).
- [15] A. P. Young, S. Knysh, and V. N. Smelyanskiy, Size Dependence of the Minimum Excitation Gap in the Quantum Adiabatic Algorithm, *Phys. Rev. Lett.* **101**, 170503 (2008).
- [16] C. Zener, Non-adiabatic crossing of energy levels, *Proc. R. Soc. London, Ser. A* **137**, 696 (1932).
- [17] N. Sinitsyn, Multiparticle Landau-Zener problem: Application to quantum dots, *Phys. Rev. B* **66**, 205303 (2002).
- [18] N. A. Sinitsyn and F. Li, Solvable multistate model of Landau-Zener transitions in cavity QED, *Phys. Rev. A* **93**, 063859 (2016).
- [19] T. Albash and D. A. Lidar, Adiabatic quantum computation, *Rev. Mod. Phys.* **90**, 015002 (2018).
- [20] E. Crosson and D. Lidar, Prospects for quantum enhancement with diabatic quantum annealing, *Nat. Rev. Phys.* **3**, 466 (2021).
- [21] E. Farhi, J. Goldstone, and S. Gutmann, A quantum approximate optimization algorithm, (2014), [arXiv:1411.4028](#).
- [22] E. Farhi and A. W. Harrow, Quantum supremacy through the quantum approximate optimization algorithm, (2016), [arXiv:1602.07674](#).
- [23] Z. Wang, S. Hadfield, Z. Jiang, and E. G. Rieffel, Quantum approximate optimization algorithm for maxcut: A fermionic view, *Phys. Rev. A* **97**, 022304 (2018).
- [24] L. Zhou, S.-T. Wang, S. Choi, H. Pichler, and M. D. Lukin, Quantum Approximate Optimization Algorithm: Performance, Mechanism, and Implementation on Near-Term Devices, *Phys. Rev. X* **10**, 021067 (2020).
- [25] M. Ohkuwa, H. Nishimori, and D. A. Lidar, Reverse annealing for the fully connected p-spin model, *Phys. Rev. A* **98**, 022314 (2018).
- [26] Y. Yamashiro, M. Ohkuwa, H. Nishimori, and D. A. Lidar, Dynamics of reverse annealing for the fully connected p-spin model, *Phys. Rev. A* **100**, 052321 (2019).
- [27] G. Passarelli, K.-W. Yip, D. A. Lidar, H. Nishimori, and P. Lucignano, Reverse quantum annealing of the p-spin model with relaxation, *Phys. Rev. A* **101**, 022331 (2020).
- [28] A. D. King *et al.*, Observation of topological phenomena in a programmable lattice of 1,800 qubits, *Nature* **560**, 456 (2018).
- [29] B. L. Altshuler, Y. Gefen, A. Kamenev, and L. S. Levitov, Quasiparticle Lifetime in a Finite System: A Nonperturbative Approach, *Phys. Rev. Lett.* **78**, 2803 (1997).
- [30] D. M. Basko, I. L. Aleiner, and B. L. Altshuler, Metal-insulator transition in a weakly interacting many-electron system with localized single-particle states, *Ann. Phys.* **321**, 1126 (2006).
- [31] I. V. Gornyi, A. D. Mirlin, and D. G. Polyakov, Interacting electrons in disordered wires: Anderson localization and low-T transport, *Phys. Rev. Lett.* **95**, 206603 (2005).
- [32] V. Oganesyan and D. A. Huse, Localization of interacting fermions at high temperature, *Phys. Rev. B* **75**, 155111 (2007).
- [33] A. Pal and D. A. Huse, Many-body localization phase transition, *Phys. Rev. B* **82**, 174411 (2010).
- [34] C. R. Laumann, A. Pal, and A. Scardicchio, Many-Body Mobility Edge in a Mean-Field Quantum Spin Glass, *Phys. Rev. Lett.* **113**, 200405 (2014).
- [35] C. Baldwin, C. Laumann, A. Pal, and A. Scardicchio, Clustering of Nonergodic Eigenstates in Quantum Spin Glasses, *Phys. Rev. Lett.* **118**, 127201 (2017).
- [36] S. Mukherjee, S. Nag, and A. Garg, Many-body localization-delocalization transition in the quantum Sherrington-Kirkpatrick model, *Phys. Rev. B* **97**, 144202 (2018).
- [37] C. Laumann, R. Moessner, A. Scardicchio, and S. L. Sondhi, Quantum Adiabatic Algorithm and Scaling of Gaps at First-Order Quantum Phase Transitions, *Phys. Rev. Lett.* **109**, 030502 (2012).
- [38] A. P. Young, Stability of the quantum Sherrington-Kirkpatrick spin glass model, *Phys. Rev. E* **96**, 032112 (2017).
- [39] A. Perdomo-Ortiz, S. E. Venegas-Andraca, and A. Aspuru-Guzik, A study of heuristic guesses for adiabatic quantum computation, *Quantum Inf. Proc.* **10**, 33 (2011).
- [40] N. Chancellor, Modernizing quantum annealing using local searches, *New J. Phys.* **19**, 023024 (2017).
- [41] V. S. Denchev, M. Mohseni, and H. Neven, *Quantum assisted optimization* (2017), international Patent Application WO 2017/189052 A1.
- [42] D. Sherrington and S. Kirkpatrick, Solvable Model of a Spin-Glass, *Phys. Rev. Lett.* **35**, 1792 (1975).
- [43] A. Crisanti, L. Leuzzi, G. Parisi, and T. Rizzo, Complexity in the Sherrington-Kirkpatrick model in the annealed approximation, *Phys. Rev. B* **68**, 174401 (2003).
- [44] A. Cavagna, I. Giardinà, and G. Parisi, Numerical Study of Metastable States in Ising Spin Glasses, *Phys. Rev. Lett.* **92**, 120603 (2004).
- [45] A. Montanari, Optimization of the Sherrington-Kirkpatrick Hamiltonian, *SIAM J. Comput.*, FOCS19 (2021).